

# Optimizing rock breaking performance: The influence of chamfer on polycrystalline diamond compact (PDC) cutters

Ju, P.<sup>a,\*</sup>

<sup>a</sup>CCTEG Xi'an Research Institute, Xi'an, P.R. China

## ABSTRACT

Research on the rock-breaking performance of the Polycrystalline Diamond Compact (PDC) cutter has primarily focused on sharp cutters, often overlooking the influence of chamfer. Notably, the design of chamfer parameters has been largely unreported. In this study, we established a theoretical model of cutting force that takes chamfer into account. We analysed the primary and secondary relationships of four factors – back rake angle, depth of cut, chamfer angle, and chamfer length – on the force of the PDC cutter. This was done through a pseudo-level orthogonal level test. A numerical simulation, based on the Smooth Particle Hydrodynamic (SPH) method, was conducted to analyse the rock-breaking force and stress distribution characteristics of PDC cutters with different chamfer angles. Combined with a drop hammer impact test, we provided an optimized design of chamfer parameters. Our findings revealed that while the chamfer had a relatively minor influence on the force of the PDC cutter, it contributed to the optimal distribution of stress on the PDC cutter. This effectively protected the cutting edge and prevented early cracks and spalls of the cutter. When the chamfer angle was less than or equal to the back rake angle, the resultant force of the PDC cutter increased with the increase of the chamfer angle. However, when the chamfer angle was greater than the back rake angle, the resultant force of the PDC cutter first increased and then slightly decreased with the increase of the chamfer angle. Additionally, the resultant force of the PDC cutter increased approximately linearly with the increase of chamfer length. When the chamfer angle of the PDC cutter was between 30° and 45°, the fluctuation of the cutting force was relatively smooth, the rock-breaking process was stable, and the cutter's impact resistance energy was relatively higher. These findings will provide valuable guidelines for the design of chamfered PDC cutters.

## ARTICLE INFO

### Keywords:

Polycrystalline diamond compact (PDC) cutter;  
Chamfer parameters;  
Optimization;  
Cutting force;  
Theoretical analysis;  
Numerical simulation;  
Smooth Particle Hydrodynamic (SPH);  
Stress characteristics

### \*Corresponding author:

[jpnt2005@163.com](mailto:jpnt2005@163.com)  
(Ju, P.)

### Article history:

Received 25 October 2023  
Revised 14 December 2023  
Accepted 15 December 2023



Content from this work may be used under the terms of the Creative Commons Attribution 4.0 International License (CC BY 4.0). Any further distribution of this work must maintain attribution to the author(s) and the title of the work, journal citation and DOI.

## 1. Introduction

In the field of petroleum and coal geological drilling, PDC bit is widely used in soft to medium hard formations, thanks to its strong rock cutting ability and high drilling efficiency. As the direct rock breaking component of PDC bit, the performance of polycrystalline diamond compact (PDC) cutter determines the drilling effect and service life of PDC bit. The PDC cutter is synthesized by polycrystalline diamond layer and cemented carbide substrate at high temperature and high pressure environment, its shape is generally cylindrical, and it has the advantages of strong self-sharpening ability, good thermal stability and strong wear resistance. However, when drilling into hard and complex formation, PDC cutters will withstand serious impact and vibration, and the problems of cutter breakage and collapse occur frequently, which seriously restrict the performance of PDC bit.

In view of the above problems, a lot of studies have been carried out. Regarding the influence of back rake angle on the performance of PDC cutter, Vusal, Zhang *et al.* pointed out that the mechanical specific energy increases as back rake angle increases [1, 2]; Adzis *et al.* raised that the larger the back rake angle, the smaller the Von Mises stress induced in the cutter, and the cutter wear rate decreases as the back rake angle increases [3]. In view of the influence of depth of cut on the rock breaking force of PDC cutter, Dai *et al.* said that at shallow depth of cut, only powdery rock chips are produced, and the fluctuation amplitude of cutting force is small, while at deep cutting depth, massive rock breakage occurs, and the fluctuation amplitude of cutting force increases significantly [4]; Li *et al.* proposed that an overall positive correlation is observed between the maximum value of the cutting force and depth of cut, the cuttings size appears to increase with the increase of depth of cut [5]; Rahmani *et al.* stated that as the increase of depth of cut, the force and force area increase gradually, and the stress on the cutter changes from tensile to compressive [6]; Joodi *et al.* put forward that with the increase of depth of cut, fractures extend deeper on the rock, and the failure mode of the rock gradually changes from ductile failure to brittle failure [7]. As for the influence of wear on the performance of PDC cutter, Iman *et al.* indicated that at a wide range of depth of cut, the frictional force on the wear flat of a blunt cutter was positively related to the angle of wear flat [8]; Zhang, Yang *et al.* stated that the cutting force, temperature change and large volume cuttings of the worn cutters are more obvious compared with the new cutter, and under the same depth, the greater the wear height is, the more obvious the force fluctuation appears [9, 10]; Liu *et al.* proposed that the wear reduces the aggressiveness of cutter, and the grinding effect of cutter on cuttings is enhanced [11].

Through previous studies, the comprehensive performance and rock breaking ability of PDC cutter have been continuously improved. In particular, it is found that although the sharp cutting edge of PDC cutter can ensure its strong attack performance, when drilling into hard and heterogeneous rock, the polycrystalline diamond layer is prone to collapse. To solve this problem, some scholars put forward the scheme of pre-chamfering the edge of polycrystalline diamond layer, with the newly added chamfered surface, the stress on the cutter is extended to a larger area, thus reducing the stress gradient on the cutting edge and enhancing the impact and wear resistance of PDC cutter [12]. Shao *et al.* pointed out that the cutting efficiency can be greatly enhanced by reducing the chamfer size, but the small chamfer size makes PDC cutters vulnerable to the premature failure [13]. Fu *et al.* proposed that the chamfer has a more significant influence on the normal than the tangential cutting force, as the chamfer becomes larger, the aggressiveness of the PDC cutter decreases considerably [14]. Akbari *et al.* put forward that at shallow cuts, a chamfered PDC cutter behaves like a cutter with higher back rake angle, the deeper the cut gets the less pronounced chamfer effect [15]. Jamaludin *et al.* expressed that the significance of the cutter geometry to the wear rate is chamfer angle, back rake angle, side rake angle and cutter diameter accordingly, the chamfer angle has the strongest correlation to the wear characteristic of PDC cutter [16].

At present, the research on the influence of chamfer on the performance of PDC cutter are mostly carried out from a macro perspective, while the specific design of the chamfer parameters has not been discussed in detailed. In this work, a theoretical cutting force model of PDC cutter considering the influence of chamfer was established; based on orthogonal design test, the primary and secondary relationship of back rake angle, depth of cut, chamfer angle and chamfer length was analysed, and the influence law of chamfer parameters on cutting force were summarized. The rock cutting simulation of PDC cutters with different chamfer angles was carried out, the influence of chamfer angle on the cutting force and stress of PDC cutter were evaluated. At the same time, the drop hammer impact test of PDC cutter was carried out, so as to guide the optimization design of chamfer parameters of PDC cutter.

## 2. Theoretical model of cutting force considering chamfer

Decomposing the force of PDC cutter with chamfer, the resultant force  $F$  of chamfered PDC cutter is composed of the resultant force  $F^c$  on the front surface of cutter and the resultant force  $F^{ch}$  on the chamfered surface of cutter. The force decomposition diagram of PDC cutter considering the chamfer is shown in Fig. 1.

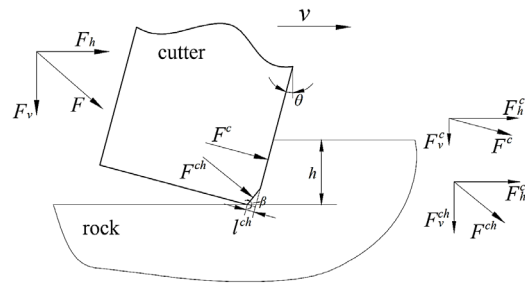


Fig. 1 Cutting force decomposition diagram of chamfered PDC cutter

According to Fig. 1, there are:

$$\begin{cases} F = \sqrt{F_h^2 + F_v^2} \\ F^c = \sqrt{F_h^{c2} + F_v^{c2}} \\ F^{ch} = \sqrt{F_h^{ch2} + F_v^{ch2}} \end{cases} \quad (1)$$

$F$  is the resultant force of chamfered PDC cutter (N);  $F_h$  and  $F_v$  denote the horizontal force and normal force of chamfered PDC cutter (N);  $F^c$  is the resultant force on the front surface of chamfered PDC cutter (N);  $F_h^c$  and  $F_v^c$  denote the horizontal force and normal force on the front surface of chamfered PDC cutter (N);  $F^{ch}$  is the resultant force on the chamfered surface of chamfered PDC cutter (N);  $F_h^{ch}$  and  $F_v^{ch}$  denote the horizontal force and normal force on the chamfered surface of chamfered PDC cutter (N).

The force of a chamfered PDC cutter can be obtained in horizontal and vertical directions respectively:

$$\begin{cases} F_h = F_h^c + F_h^{ch} \\ F_v = F_v^c + F_v^{ch} \end{cases} \quad (2)$$

According to reference [17], it can be obtained:

$$\begin{cases} F_h^c = \varepsilon A^c \\ F_v^c = \tan(\theta + \varphi) \varepsilon A^c \end{cases} \quad (3)$$

$$\begin{cases} F_h^{ch} = \varepsilon A^{ch} \\ F_v^{ch} = \tan(\theta + \varphi) \varepsilon A^{ch} \end{cases} \quad (4)$$

$A^c$  is the contact area between the front surface and the rock ( $\text{m}^2$ );  $A^{ch}$  is the contact area between the chamfered surface and the rock, ( $\text{m}^2$ );  $\theta$  is the back rake angle (rad);  $\varepsilon$  is the intrinsic specific energy of rock (Pa);  $\varphi$  is the internal friction angle of rock (rad).

Substituting Eq. 3 and Eq. 4 into Eq. 1 and Eq. 2, the forces on the front surface and chamfered surface can be obtained, and the resultant force of chamfered PDC cutter can be calculated.

It is important to note that, the contact area  $A^c$  and  $A^{ch}$  are related to the relationship between chamfer angle and back rake angle, the calculation of the contact area needs to be considered from the following three cases respectively.

#### (1) Chamfer angle is greater than back rake angle

When the chamfer angle is greater than back rake angle, the chamfered surface of the PDC cutter is in full contact with the rock. The contact state and contact area between the PDC cutter and the rock are shown in Fig. 2.

According to Fig. 2, it can be obtained:

$$\begin{cases} A^c = S_{secOEF} - S_{triOEF} = \frac{1}{2}(\angle EOF) \cdot |OB|^2 - \frac{1}{2}|OE| \cdot |OF| \cdot \sin(\angle EOF) \\ A^{ch} = S_{secOPQ} - S_{secOEF} = \frac{1}{2}(\angle EOF) \cdot |OP|^2 - \frac{1}{2}(\angle EOF) \cdot |OB|^2 \end{cases} \quad (5)$$

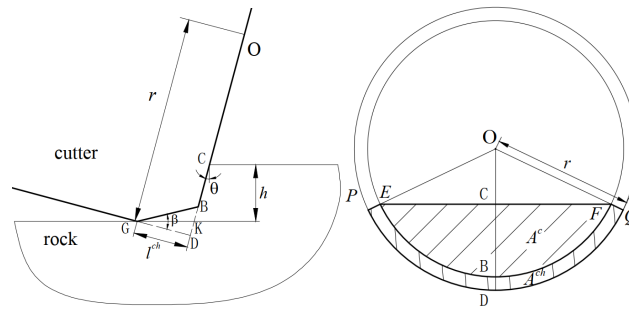


**Fig. 2** Diagram of the contact state and contact area between the PDC cutter and the rock when chamfer angle is greater than back rake angle

The  $\angle EOF$  is expressed in radians.

$$\begin{aligned} \angle EOF &= 2 \arccos \left( \frac{|OC|}{|OF|} \right) = 2 \arccos \left( \frac{|OD| - |BD| - |BC|}{|OB|} \right) \\ &= 2 \arccos \left[ \frac{|OD| - |BD| - \left( \frac{h}{\cos \theta} - |BK| \right)}{|OD| - |BD|} \right] = 2 \arccos \left\{ \frac{|OD| - |BD| - \left[ \frac{h}{\cos \theta} - (|BD| - |DK|) \right]}{|OD| - |BD|} \right\} \quad (6) \\ &= 2 \arccos \left\{ \frac{r - l^{ch} \tan \beta - \left[ \frac{h}{\cos \theta} - (l^{ch} \tan \beta - l^{ch} \tan \theta) \right]}{r - l^{ch} \tan \beta} \right\} = 2 \arccos \left( \frac{r - \frac{h}{\cos \theta} - l^{ch} \tan \theta}{r - l^{ch} \tan \beta} \right) \end{aligned}$$

$$|OE| = |OF| = |OB| = |OD| - |BD| = r - l^{ch} \tan \beta \quad (7)$$

where  $r$  is the radius of chamfered PDC cutter (m);  $h$  is the depth of cut (m);  $\beta$  is the chamfer angle (rad);  $l^{ch}$  is the chamfer length (m).

Substituting Eq. 6 and Eq. 7 into Eq. 5,  $A^c$  and  $A^{ch}$  can be expressed:

$$\begin{cases} A^c = (r - l^{ch} \tan \beta)^2 \cdot \left\{ \arccos \left( \frac{r - \frac{h}{\cos \theta} - l^{ch} \tan \theta}{r - l^{ch} \tan \beta} \right) - \frac{1}{2} \sin \left[ 2 \arccos \left( \frac{r - \frac{h}{\cos \theta} - l^{ch} \tan \theta}{r - l^{ch} \tan \beta} \right) \right] \right\} \\ A^{ch} = \arccos \left( \frac{r - \frac{h}{\cos \theta} - l^{ch} \tan \theta}{r - l^{ch} \tan \beta} \right) \cdot [r^2 - (r - l^{ch} \tan \beta)^2] \end{cases} \quad (8)$$

Substituting Eq. 8 into Eq. 3 and Eq. 4, the horizontal force and normal force acting on the front surface and chamfered surface of PDC cutter can be obtained.

*(2) Chamfer angle is equal to back rake angle*

Fig. 3 shows the contact state and contact area between the PDC cutter and the rock when the chamfer angle is equal to back rake angle, at this time, the chamfered line BG showed in Fig. 3 is parallel to the horizontal direction.

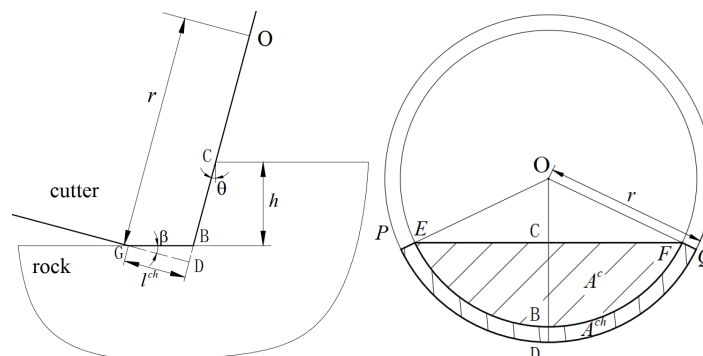


**Fig. 3** Diagram of the contact state and contact area between the PDC cutter and rock when chamfer angle is equal to back rake angle

According to Fig. 3, it can be obtained:

$$\begin{cases} F_h^{ch} = \mu F_v^{ch} \\ F_v^{ch} = \tan(\theta + \varphi) \varepsilon A^{ch} \end{cases} \quad (9)$$

where  $\mu$  is the friction coefficient of rock.

$$\begin{cases} A^c = S_{secOEF} - S_{triOEF} = \frac{1}{2}(\angle EOF) \cdot |OB|^2 - \frac{1}{2}|OE| \cdot |OF| \cdot \sin(\angle EOF) \\ A^{ch} = S_{secOPQ} - S_{secOEF} = \frac{1}{2}(\angle EOF) \cdot |OP|^2 - \frac{1}{2}(\angle EOF) \cdot |OB|^2 \end{cases} \quad (10)$$

$$\begin{aligned} \angle EOF &= 2 \arccos\left(\frac{|OC|}{|OF|}\right) = 2 \arccos\left(\frac{|OD| - |BD| - |BC|}{|OB|}\right) \\ &= 2 \arccos\left(\frac{|OD| - |BD| - |BC|}{|OD| - |BD|}\right) = 2 \arccos\left(\frac{r - l^{ch} \tan \beta - \frac{h}{\cos \theta}}{r - l^{ch} \tan \beta}\right) \end{aligned} \quad (11)$$

$$|OE| = |OF| = |OB| = |OD| - |BD| = r - l^{ch} \tan \beta \quad (12)$$

Substituting Eq. 11 and Eq. 12 into Eq. 10,  $A^c$  and  $A^{ch}$  can be expressed:

$$\begin{cases} A^c = (r - l^{ch} \tan \beta)^2 \cdot \left\{ \arccos\left(\frac{r - l^{ch} \tan \beta - \frac{h}{\cos \theta}}{r - l^{ch} \tan \beta}\right) - \frac{1}{2} \sin\left[2 \arccos\left(\frac{r - l^{ch} \tan \beta - \frac{h}{\cos \theta}}{r - l^{ch} \tan \beta}\right)\right] \right\} \\ A^{ch} = \arccos\left(\frac{r - l^{ch} \tan \beta - \frac{h}{\cos \theta}}{r - l^{ch} \tan \beta}\right) \cdot [r^2 - (r - l^{ch} \tan \beta)^2] \end{cases} \quad (13)$$

Substituting Eq. 13 into Eq. 3 and Eq. 9, the horizontal force and normal force acting on the front surface and chamfered surface of PDC cutter can be obtained.

(3) Chamfer angle is less than back rake angle

When the chamfer angle is less than back rake angle, in an ideal state, the chamfered surface of the PDC cutter does not contact with the rock. The contact state and contact area between the PDC cutter and the rock are shown in Fig. 4.

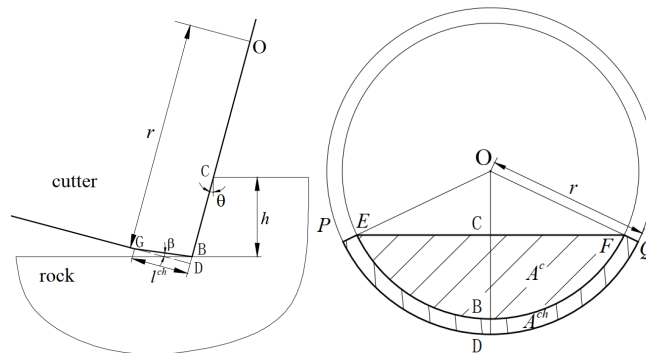


Fig. 4 Diagram of the contact state and contact area between the PDC cutter and rock when chamfer angle is equal to back rake angle

According to Fig. 4, it can be obtained:

$$F_h^{ch} = F_v^{ch} = 0 \quad (14)$$

$$A^c = S_{secOEF} - S_{triOEF} = \frac{1}{2}(\angle EOF) \cdot |OB|^2 - \frac{1}{2}|OE| \cdot |OF| \cdot \sin(\angle EOF) \quad (15)$$

$$\begin{aligned} \angle EOF &= 2 \arccos\left(\frac{|OC|}{|OF|}\right) = 2 \arccos\left(\frac{|OD| - |BD| - |BC|}{|OB|}\right) \\ &= 2 \arccos\left(\frac{|OD| - |BD| - |BC|}{|OD| - |BD|}\right) = 2 \arccos\left(\frac{r - l^{ch} \tan \beta - \frac{h}{\cos \theta}}{r - l^{ch} \tan \beta}\right) \end{aligned} \quad (16)$$

$$|OE| = |OF| = |OB| = |OD| - |BD| = r - l^{ch}\tan \beta \tag{17}$$

Substituting Eq. 16 and Eq. 17 into Eq. 15,  $A^c$  can be expressed:

$$A^c = (r - l^{ch}\tan \beta)^2 \cdot \left\{ \arccos \left( \frac{r - l^{ch}\tan \beta - \frac{h}{\cos \theta}}{r - l^{ch}\tan \beta} \right) - \frac{1}{2} \sin \left[ 2 \arccos \left( \frac{r - l^{ch}\tan \beta - \frac{h}{\cos \theta}}{r - l^{ch}\tan \beta} \right) \right] \right\} \tag{18}$$

Substituting Eq. 18 into Eq. 3, the horizontal force and normal force acting on the front surface of PDC cutter can be obtained.

### 3. Primary and secondary factors affecting the force of cutter

Based on previous research, it is known that back rake angle and depth of cut have significant influence on the force of cutter [18-23]. Therefore, combined with the focus of this work, the orthogonal design test of four factors, i.e. back rake angle, depth of cut, chamfer angle and chamfer length, was established, the influence degree of the four factors on the force of cutter was analysed according to the above established equations.

#### 3.1 Pseudo-level orthogonal test design

Table 1 is the orthogonal design level table of the factors affecting the force of cutter.

According to Table 1, orthogonal test table  $L_{81}(4^9)$  was selected for the pseudo-level design of the four factors. According to experience, the designed back rake angle is generally between 10 and 20° [24, 25], the depth of cut that the bit drill into the rock per turn is generally between 2 and 3 mm [26, 27], therefore, in the pseudo-level orthogonal test table, the second, third and fourth levels (10°, 15° and 18°) of the back rake angle were repeated once respectively, and the third, fourth and fifth levels (2 mm, 2.5 mm, 3 mm) of the depth of cut were repeated once respectively. Because the influence of chamfer length on the force of cutter is unknown, a random repetition of the chamfer length level was performed. Based on this, the pseudo-level orthogonal test table was designed, and the parameters in the table were substituted into the equations derived in Section 2, the results are shown in Table 2.

**Table 1** Orthogonal design level table of the factors affecting the force of cutter

Factor Level	A Back rake angle (°)	B Cutting depth (°)	C Chamfer angle (°)	D Chamfer length (°)
1	5	1	5	0.2
2	10	1.5	10	0.3
3	15	2	15	0.4
4	18	2.5	18	0.5
5	20	3	20	
6	25	3.5	25	
7			30	
8			45	
9			60	

**Table 2** Pseudo-level orthogonal test level table of the force influencing factors and the results

No.	Back rake angle (°)	Depth of cut (mm)	Chamfer angle (°)	Chamfer length (mm)	Resultant force on front surface (N)	Resultant force on chamfered surface (N)	Resultant force of PDC cutter (N)
1	25	1.5	60	0.3	878.381	241.014	1119.395
2	5	2.5	45	0.4	1695.374	256.402	1951.776
3	10	3	45	0.2	1603.419	130.957	1734.376
4	18	1.5	25	0.4	737.354	130.366	867.719
5	15	3.5	18	0.2	2378.183	70.499	2448.682
6	18	2	60	0.4	978.008	297.613	1275.620
7	5	2	15	0.3	828.478	53.342	881.820
8	15	2	45	0.3	963.713	172.976	1136.689
9	18	2	18	0.3	1169.110	80.727	1249.067
10	15	1	10	0.5	388.434	0.000	388.434
11	18	2.5	15	0.2	1618.022	0.000	1618.022
12	15	2.5	20	0.3	1457.285	97.073	1554.358
13	15	1.5	18	0.2	700.775	44.704	745.479

**Table 2** (continuation)

No.	Back rake angle (°)	Depth of cut (mm)	Chamfer angle (°)	Chamfer length (mm)	Resultant force on front surface (N)	Resultant force on chamfered surface (N)	Resultant force of PDC cutter (N)
14	20	3	5	0.2	2245.877	0.000	2245.877
15	10	2	60	0.2	848.894	126.749	975.643
16	18	2.5	5	0.5	1619.379	0.000	1619.379
17	18	1	20	0.3	420.950	64.812	485.761
18	18	3	5	0.3	2102.773	0.000	2102.773
19	25	3.5	5	0.3	3363.261	0.000	3363.261
20	18	3	10	0.5	2091.386	0.000	2091.386
21	18	3	25	0.2	2073.736	95.201	2168.936
22	18	3	60	0.4	1847.717	377.403	2225.120
23	10	2	25	0.5	855.799	155.301	1011.099
24	5	3	60	0.5	1225.042	348.676	1573.718
25	10	1.5	5	0.3	625.856	0.000	625.856
26	15	2.5	5	0.5	1482.830	0.000	1482.830
27	25	2.5	10	0.4	2083.419	0.000	2083.419
28	20	3.5	10	0.3	2771.957	0.000	2771.957
29	25	2	20	0.4	1502.580	0.000	1502.580
30	10	3.5	20	0.5	2021.925	173.535	2195.459
31	18	2.5	45	0.5	1414.735	348.157	1762.892
32	18	3.5	15	0.4	2593.402	0.000	2593.402
33	25	1	45	0.2	511.444	108.000	619.444
34	18	2.5	20	0.2	1612.969	69.961	1682.929
35	10	1	15	0.4	326.428	53.884	380.312
36	15	3	10	0.4	1918.500	0.000	1918.500
37	15	3	30	0.3	1844.863	155.515	2000.378
38	15	3.5	45	0.4	2180.744	314.904	2495.649
39	10	3	18	0.5	1632.464	144.143	1776.607
40	20	2.5	15	0.2	1727.147	0.000	1727.147
41	25	2.5	25	0.5	2054.058	291.706	2345.709
42	25	3	18	0.5	2676.756	0.000	2676.756
43	20	2	45	0.5	1081.393	324.940	1406.333
44	10	2.5	10	0.3	1310.027	36.491	1345.110
45	10	3.5	60	0.2	1976.607	174.213	2150.819
46	15	2.5	60	0.3	1312.954	237.843	1550.797
47	15	3	30	0.4	1816.806	206.570	2023.375
48	10	3	45	0.3	1552.690	194.604	1747.294
49	10	1	18	0.4	316.120	63.660	379.781
50	10	3	15	0.3	1676.193	72.944	1749.138
51	20	3	20	0.3	2227.834	121.871	2349.031
52	5	3	20	0.4	1458.881	116.273	1575.154
53	18	1	30	0.3	391.643	92.531	484.174
54	20	2.5	18	0.4	1715.850	0.000	1715.850
55	10	2.5	30	0.2	1257.302	84.328	1341.630
56	18	2	10	0.2	1175.170	0.000	1175.170
57	5	2.5	18	0.3	1140.615	71.677	1212.292
58	10	2	10	0.3	949.537	32.402	980.695
59	15	2	5	0.4	1075.850	0.000	1075.850
60	10	2.5	25	0.4	1225.452	141.568	1367.020
61	20	2	25	0.3	1230.262	121.130	1351.392
62	5	1	5	0.2	313.160	6.234	318.981
63	5	1.5	10	0.2	558.197	20.674	578.871
64	15	3	25	0.2	1889.151	88.195	1977.347
65	5	2	30	0.5	724.446	164.589	889.035
66	18	3.5	30	0.5	2474.827	304.077	2778.904
67	20	1	60	0.5	296.278	252.482	548.761
68	5	3.5	25	0.3	1829.778	117.601	1947.379
69	15	1	25	0.3	361.907	72.841	434.748
70	25	3	15	0.3	2696.483	0.000	2696.483
71	10	2	5	0.4	950.940	0.000	950.940
72	15	2	15	0.5	1067.024	98.846	1164.149
73	20	1.5	30	0.4	774.430	162.056	936.486
74	10	1.5	20	0.5	569.941	108.467	678.408
75	15	2	20	0.2	1061.781	57.489	1119.269
76	15	1.5	15	0.5	702.100	84.981	785.639
77	25	2	30	0.2	1501.723	112.019	1613.742
78	10	2.5	30	0.3	1228.481	125.641	1354.122
79	18	1.5	45	0.3	682.543	159.383	841.926

### 3.2 Multi-factor variance analysis

In the drilling process, rock breaking force is simultaneously affected by four factors: back rake angle, depth of cut, chamfer angle and chamfer length. Therefore, taking the resultant force on the front surface, the resultant force on the chamfered surface, and the resultant force of PDC cutter as targets respectively, the data in Table 2 were analysed by multi-factor variance method [28]. Taking the resultant force on the front surface of PDC cutter as object, the varication analysis results of each factor are shown in Table 3.

**Table 3** Multi-factor variance analysis with the object of the resultant force on the front surface of PDC cutter

Source of variation	Sum of deviation square	Freedom	Mean square	Value of F
Factor A (back rake angle)	12303791.19	5	2460758.239	2.145812091
Factor B (depth of cut)	53507230.5	5	10701446.1	9.331795407
Factor C (chamfer angle)	1508953.542	8	188619.1928	0.164478305
Factor D (chamfer length)	3924539.023	3	1308179.674	1.140749107
Factor E (error)	9174179.787	8	1146772.473	

According to Table 3, from high to low, the influence degree of each factor on the resultant force of PDC cutter is as follows: depth of cut, back rake angle, chamfer length and chamfer angle. The depth of cut shows the most significant effect on the resultant force of front surface.

Taking the resultant force on the chamfered surface of PDC cutter as object, the varication analysis results of each factor are shown in Table 4.

**Table 4** Multi-factor variance analysis with the object of the resultant force on the chamfered surface of PDC cutter

Source of variation	Sum of deviation square	Freedom	Mean square	Value of F
Factor A (back rake angle)	99076.91606	5	19815.38321	1.331109649
Factor B (depth of cut)	109763.2665	5	21952.6533	1.474681984
Factor C (chamfer angle)	551868.6539	8	68983.58174	4.634011378
Factor D (chamfer length)	69317.13208	3	23105.71069	1.552139271
Factor E (error)	119090.9147	8	14886.36434	

According to Table 4, from high to low, the influence degree of each factor on the resultant force of PDC cutter is as follows: chamfer angle, chamfer length, depth of cut and back rake angle. The chamfer angle shows the most significant effect on the resultant force of chamfered surface.

Taking the resultant force of PDC cutter as object, the varication analysis results of each factor are shown in Table 5.

**Table 5** Multi-factor variance analysis with the object of the resultant force of PDC cutter

Source of variation	Sum of deviation square	Freedom	Mean square	Value of F
Factor A (back rake angle)	14082530.17	5	2816506.033	2.320851882
Factor B (depth of cut)	57888672.68	5	11577734.54	9.540262536
Factor C (chamfer angle)	568633.273	8	71079.15912	0.058570512
Factor D (chamfer length)	4160716.972	3	1386905.657	1.142835331
Factor E (error)	9708524.89	8	1213565.611	

According to Table 5, from high to low, the influence degree of each factor on the resultant force of PDC cutter is as follows: depth of cut, back rake angle, chamfer length and chamfer angle. The depth of cut shows the most significant effect on the resultant force of PDC cutter, while the chamfer angle and chamfer length have no significant effect.

Through multi-factor variance analysis, it can be obtained that, the depth of cut plays a major role in the force of PDC cutter, followed by the back rake angle. The chamfer shows the significant effect on the resultant force of chamfered surface, it mainly affects the stress distribution of the PDC cutter, that is, the chamfer mainly affects the wear and impact resistance of the cutter.



## 4. Influence of chamfer parameters on the force of PDC cutter

Although the chamfer contributes minimally to the force of the PDC cutter, it is essential to examine the influence of the chamfer parameters on the force. This examination will provide guidance for the design of chamfer parameters. Based on the equations established in Section 2, the influence of the chamfer angle and chamfer length on the force of the PDC cutter was analysed separately.

### 4.1 Influence of chamfer angle on the force of PDC cutter

Based on previous research, fixing the back rake angle  $15^\circ$  and the depth of cut 0.3 mm unchanged [29, 30], the influence law of chamfer angle on the force of PDC cutter with different chamfer lengths was analysed. Figs. 5, 6 and 7 show the variation characteristics of the resultant force on front surface, the resultant force on chamfered surface and the resultant force of PDC cutter with chamfer angle respectively.

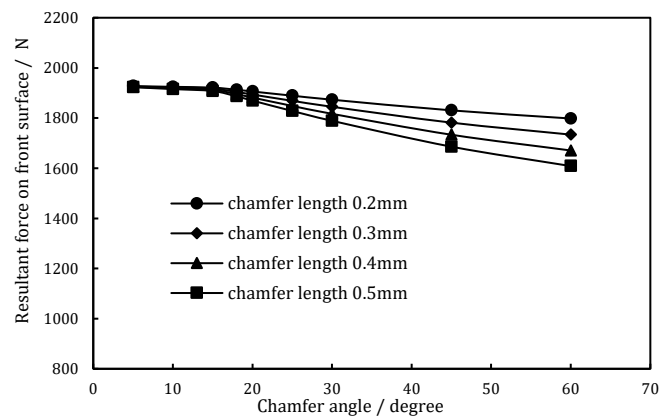


Fig. 5 Variation curve of the resultant force on front surface of PDC cutter with chamfer angle

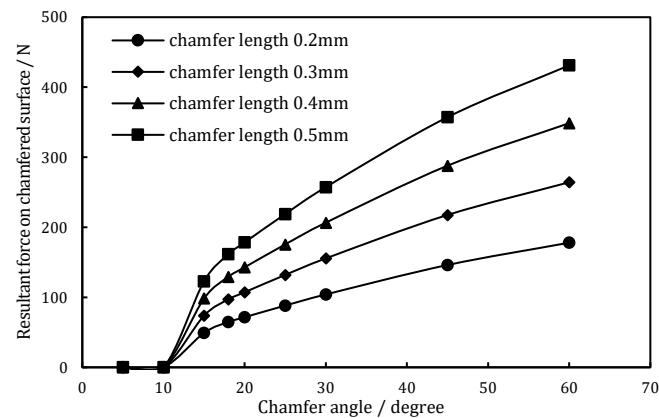


Fig. 6 Variation curve of the resultant force on chamfered surface of PDC cutter with chamfer angle

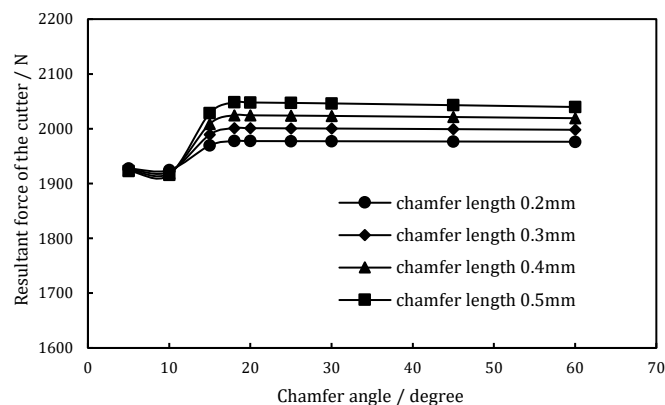


Fig. 7 Variation curve of the resultant force of PDC cutter with chamfer angle

According to Figs. 5, 6 and 7, when the chamfer angle is small (chamfer angle not greater than back rake angle), the chamfer angle appears almost no influence on the resultant force on both front and chamfered surface, while the resultant force of PDC cutter increases significantly with the increase of chamfer angle. When the chamfer angle is greater than back rake angle, with the increase of chamfer angle, the resultant force on the front surface decreases linearly, while the resultant force on chamfered surface increases approximately linearly, and the larger the chamfer length, the faster the reduction or increase rate. The resultant force of PDC cutter increases first and then decreases slightly with the increase of chamfer angle, the decreasing trend can be ignored when the chamfer length is small.

#### 4.2 Influence of chamfer length on the force of PDC cutter

Fixing the back rake angle  $15^\circ$  and the depth of cut 0.3 mm unchanged, the influence of chamfer length on the force of PDC cutter with different chamfer angles was analysed. Figs. 8, 9 and 10 show the variation characteristics of the resultant force on front surface, the resultant force on chamfered surface and the resultant force of PDC cutter with chamfer length respectively.

According to Figs. 8, 9 and 10, when the chamfer angle is small (chamfer angle not greater than back rake angle), the chamfer length appears almost no influence on both the resultant force on front surface, chamfered surface and the PDC cutter. When chamfer angle is greater than back rake angle, with the increase of chamfer length, the resultant force on the front surface decreases linearly, while the resultant force on chamfered surface increases approximately linearly, and the greater the chamfer angle, the faster the reduction or increase rate. The resultant force of PDC cutter increases linearly with the increase of chamfer length, and the amplitude of linear increase is almost unchanged under different chamfer angles.

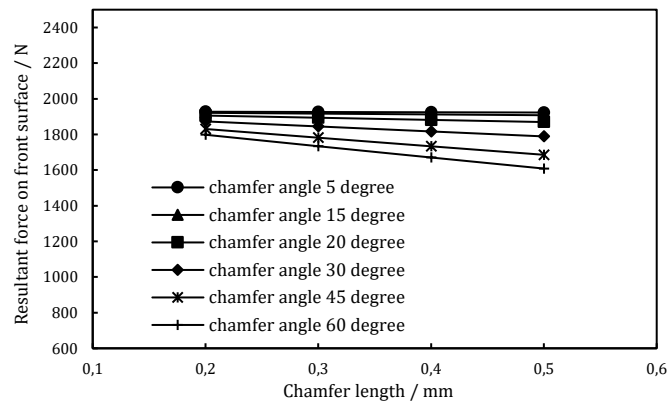


Fig. 8 Variation curve of the resultant force on front surface of PDC cutter with chamfer length

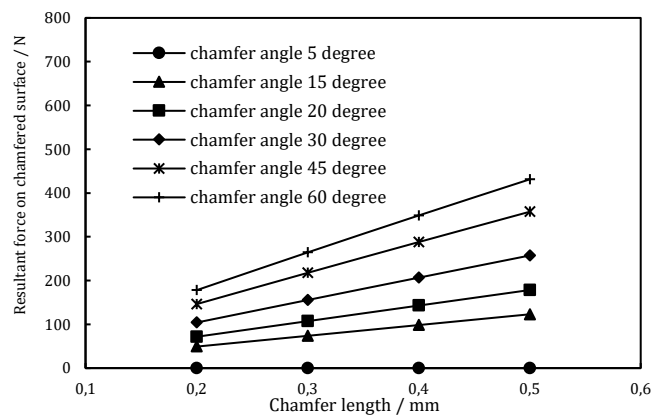


Fig. 9 Variation curve of the resultant force on chamfered surface of PDC cutter with chamfer length

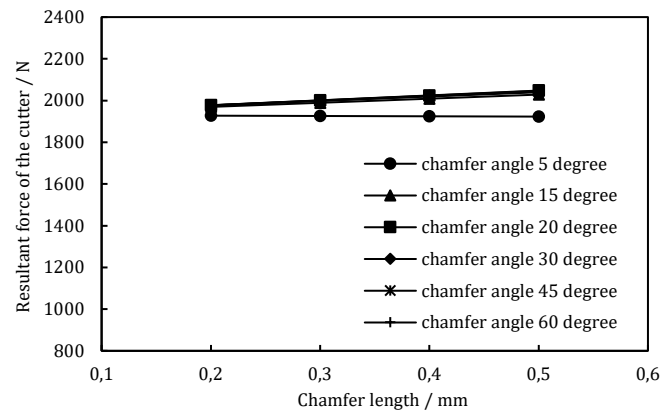


Fig. 10 Variation curve of the resultant force of PDC cutter with chamfer length

## 5. Rock breaking simulation of PDC cutters with different chamfer angles

It is beneficial to improve the stress distribution by chamfering the PDC cutter, but it is difficult to observe the stress state of the PDC cutter through theoretical and experimental analysis. So in this work, numerical simulation based on Smooth Particle Hydrodynamic (SPH) method was used to reveal the rock breaking characteristics and stress state of PDC cutters with different chamfer angles.

### 5.1 Simulation model

The SPH is a meshless continuum mechanics method, in which the computation domain is discretized into a series of interacting particles. Its good adaptive characteristics make it can deal with the problems of large deformation and post-instability well, so can effectively avoid the mesh distortion caused by rock breaking [31, 32]. In this work, the following assumptions were made: (1) the rocks were continuous, homogeneous and isotropic; (2) the influence of temperature and fluid was ignored; (3) regardless of repeated breaking, the rock unit was deleted immediately after being broken.

Drucker-Prager model was used to simulate the constitutive relation of rock [33]. In this model, the formation and peeling process of cuttings can be represented by setting shear failure criterion, and the shear failure of rock can be simulated well. The failure equivalent plastic strain was defined as the criterion of rock damage. When the equivalent plastic strain of rock was equal to the failure plastic strain, the rock element was broken and deleted [24]. The cutter was represented by an elastic model, which can consider the wear of the cutter. Table 6 shows the material parameters of the cutter and the rock.

The size of rock was  $40 \times 30 \times 30$  mm, and it was modelled by SPH particles, the particle size was 0.8 mm. The size of cutter was  $\Phi 13.44 \times 8$  mm, and it was modelled by hexahedral element, the mesh size was 0.4 mm. The rock was completely fixed, the cutter cut the rock linearly along the Y axis at a speed of 100 m/h, and the depth of cut was set 3 mm unchanged. Fig. 11 shows the 3D model of linear cutting rock by PDC cutter.

The idea of unit erosion algorithm was taken for reference to deal with the failure of SPH rock particles, the rock particles were deemed to be invalid when the damage variable of rock particles reach the critical value, the rock particles were deleted, but the mass and momentum of the failed particles were still retained, thus ensuring the conservation of mass and momentum of the system.

Table 6 Material parameters of the cutter and rock

	Density ( $\text{kg}\cdot\text{m}^{-3}$ )	Elastic modulus (GPa)	Poisson's ratio	Compressive strength (MPa)	Shear strength (MPa)	Cohesion (MPa)	Internal friction angle ( $^{\circ}$ )
Cutter	3560	850	0.07				
Rock	2500	40	0.27	75	10.0	27.2	35.0

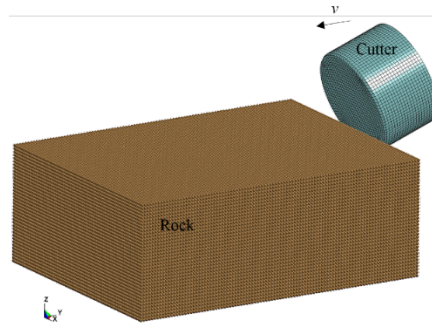


Fig. 11 3D model of linear cutting rock by PDC cutter

According to the analysis in Section 2, the relationship between the chamfer angle and back rake angle determines the contact state between PDC cutter and the rock. Therefore, in this simulation, the rock breaking characteristics of PDC cutters with different chamfer angles under different back rake angles were analysed. Table 7 shows the parameters of PDC cutter in the simulation.

Table 7 Parameters of PDC cutter

Cutter size (mm)	Chamfer length (mm)	Back rake angle (°)	Chamfer angle (°)
Φ 13.44 × 8	0.3	15	15
			30
			45
			60
		18	15
			30
			45
			60
		20	15
			30
			45
			60

### 5.2 Rock breaking force

Fig. 12 shows the stress nephogram of rock and force curve of PDC cutter during rock breaking process. As can be observed, the rock particles were broken under the shear and extrusion actions of PDC cutter, an arc-shaped crushing pit was formed, the maximum stress on the rock was located in the front surface of the cutting edge, which took the shape of an arc belt. When the rock breaking process was stable, the cutting force, axial force and lateral force all fluctuated with time, and the collapse failure of rock particles was reflected in the sudden decrease of cutting force. In this work, all the analysis are based on the stable cutting stage, and the lateral force is relatively small, so it is ignored.

Fig. 13 shows the force curves of PDC cutters with different chamfer angles under different back rake angles. As can be observed, both the cutting force and the axial force increase with the increase of back rake angle, which is consistent with the conclusion in reference 34 [34]. Under all the back rake angles, the cutting force and axial force present the same changing law with the increase of chamfer angle, that is, a trend of first increasing and then slightly decreasing, and the decrease amplitude is very small (which is consistent with the conclusion obtained in Fig. 7). Moreover, the larger the back rake angle is, the more significant the change is. When the back rake angle is 15°, the cutting force and axial force show little difference with the chamfer angle. When the chamfer angle is less than back rake angle, the influence of chamfer angle on cutting force and axial force is more obvious, while when the chamfer angle is larger than back rake angle, the influence of chamfer angle on cutting force and axial force is very small, which can be almost ignored.

According to Fig. 12, the cutting force fluctuates up and down around a certain value in the process of rock breaking, the more severe the fluctuation, the greater the possibility of vibration damage to the PDC cutter. The cutting force difference coefficient is used to evaluate the severity of the fluctuation, which is defined as the ratio between the standard deviation of cutting force

and the mean value of cutting force. The smaller the cutting force difference coefficient is, the gentler the fluctuation of the cutting force is. Fig. 14 shows the cutting force difference coefficient curves of PDC cutters with different chamfer angles under different back rake angles.

It can be seen from Fig. 14, when the chamfer angle is between 30° and 45°, the cutting force difference coefficient is small, and the rock breaking process is relatively stable. Similar conclusions can be drawn at different back rake angles.

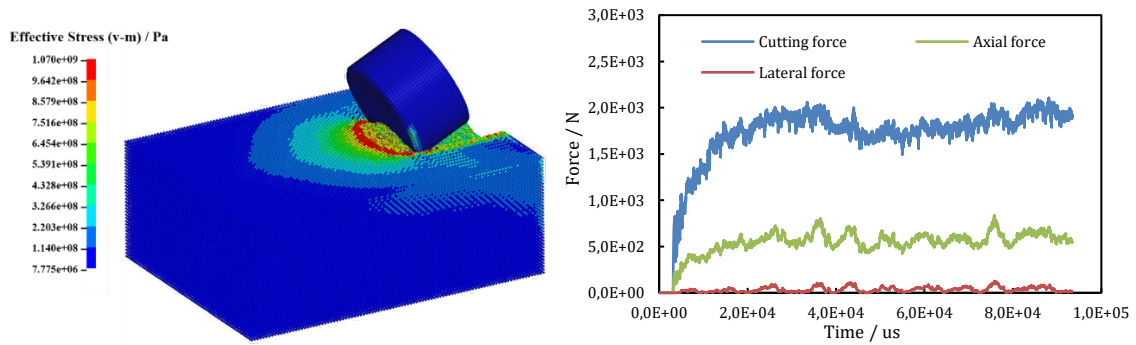


Fig. 12 Stress nephogram of rock and force curve of PDC cutter

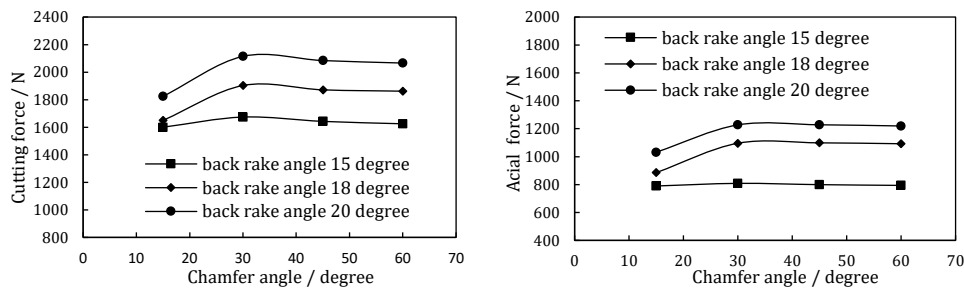


Fig. 13 Force curves of PDC cutters with different chamfer angles under different back rake angles

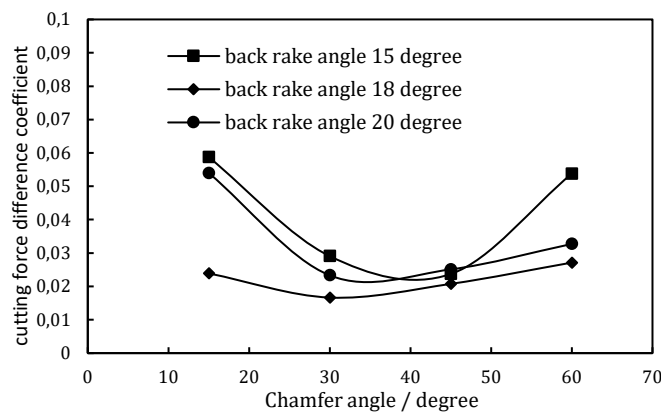
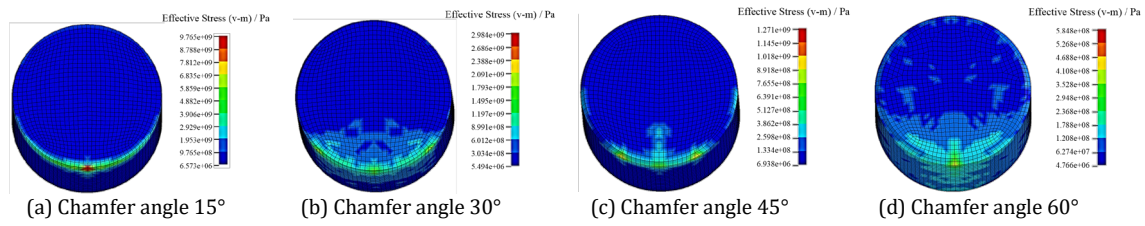


Fig. 14 Cutting force difference coefficient curves of PDC cutters with different chamfer angles

### 5.3 Stress distribution characteristic of PDC cutter

Fig. 15 shows the stress distribution nephogram of PDC cutters with different chamfer angles at a back rake angle of 25°. With the increase of chamfer angle, the maximum stress on the PDC cutter decreases gradually, and the stress distribution area expands from the cutting edge to a larger area. Specifically, when the chamfer angle is 15°, the surface stress on the PDC cutter is concentrated in the part where the lower edge of the PDC cutter contacts with the rock. At this time, the stress on the lower of the cutting edge is concentrated, and the collapse failure of the cutting edge is easy to occur. When the chamfer angle is increased to 60°, the surface stress on the PDC cutter spreads to a larger area, which effectively protects the cutting edge, prevents the occurrence of early cracks and spalls of the polycrystalline diamond layer.



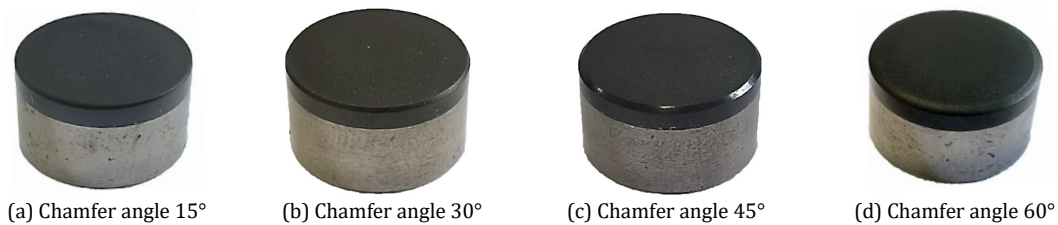
**Fig. 15** Stress distribution nephogram of PDC cutters with different chamfer angles

### 6. Impact resistance test of PDC cutters with different chamfer angles

Drop hammer impact tests of PDC cutters with chamfer angles of 15°, 30°, 45° and 60° were carried out to further verify the influence of chamfer on the impact resistance of PDC cutter. Fig. 16 shows the photos of PDC cutters with different chamfer angles, and the cutter sizes are  $\Phi 13.44 \times 8$  mm.

The drop hammer impact device was used in the test (shown as Fig. 17), PDC cutters were fixed on the punch head with a back rake angle of 20°. The mould steel was continuously impacted by the PDC cutter with a given energy, the hardness of the mould steel was HRC58-62. Every time the punch impacted, the mould steel rotated by 10°, so to ensure the PDC cutter can impact the undamaged mould steel plane every time.

The impact energy was loaded in a step-by-step energy mode. Starting from 10 J impact energy for 10 times, the energy was increased step-by-step for 20 J impact energy for 10 times, 30 J impact energy for 10 times and 40 J impact energy for 10 times, the test was stopped once the polycrystalline diamond layer was damaged. The total impact energy that the PDC cutter can withstand was calculated according to the sum of the single impact energy. Two pieces of each chamfered cutter were tested, the average of the two test results was taken as the final impact resistance energy of the chamfered cutter. Table 8 shows the cumulative average impact energy of the PDC cutter with different chamfer angles.





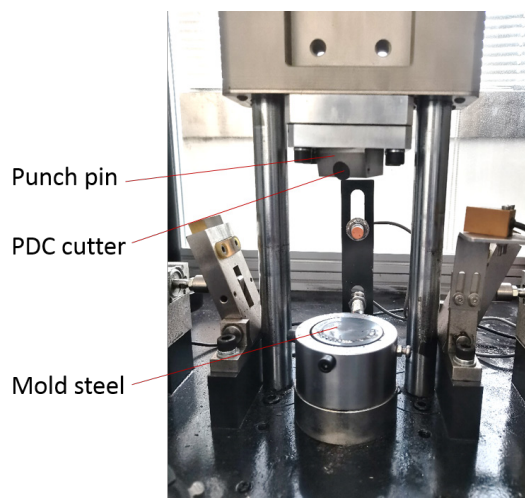


**Fig. 16** Photos of PDC cutters with different chamfer angles



**Fig. 17** Photo of drop hammer impact device

**Table 8** Impact test data of PDC cutters

PDC cutter	Number of impact				Cumulative average impact energy/ J	Damage morphology
	10J	20J	30J	40J		
Chamfer angle 15°	10	10	2	/	500	
	10	10	10	1		
Chamfer angle 30°	10	10	10	1	605	
	10	10	9	/		
Chamfer angle 45°	10	10	10	2	740	
	10	10	10	5		
Chamfer angle 60°	10	10	10	10	920	
	10	10	10	6		

According to Table 8, when the impact energy was less than 20 J, all the PDC cutters were intact. When the impact energy was increased to 30 J, the whole polycrystalline diamond layer collapsed on one PDC cutter with chamfer angle of 15°, and the side edge of polycrystalline diamond layer broke on one PDC cutter with chamfer angle of 30°. When the impact energy was increased to 40 J, the main damage forms of all the PDC cutters were the whole collapsing of polycrystalline diamond layer, the upper surface of polycrystalline diamond layer cracked on one PDC cutter with chamfer angle of 45°, and the side edge of polycrystalline diamond layer broke on one PDC cutter with chamfer angle of 60°. Considering the impact energy and damage morphology comprehensively, the impact resistance of PDC cutters with chamfer angle of 45° and 60° were superior, and this was in good agreement with the simulation results.

## 7. Conclusion

In this study, theoretical model of cutting force considering chamfer was established, the primary and secondary relationship of four factors – back rake angle, depth of cut, chamfer angle and chamfer length – on the force of PDC cutter was analysed through pseudo-level orthogonal level test. The depth of cut played a major role in the resultant force on front surface and the PDC cutter, followed by the back rake angle. The chamfer angle showed the most significant effect on the resultant force on chamfered surface.

The influence of the chamfer parameters on the force of PDC cutter was analysed. When the chamfer angle was small (chamfer angle not greater than back rake angle), the chamfer angle and chamfer length appeared almost no influence on the resultant force on both front surface and chamfered surface of PDC cutter, while the resultant force of PDC cutter increased significantly with the increase of chamfer angle. When chamfer angle was greater than back rake angle, with the increase of chamfer angle and chamfer length, the resultant force on the front surface decreased linearly, while the resultant force on the chamfered surface increased approximately linearly; for the resultant force of PDC cutter, it increased first and then decreased slightly with the increase of chamfer angle, also it increased linearly with the increase of chamfer length.

Numerical simulation based on SPH method was carried out to analyse the rock breaking characteristics of PDC cutters with different chamfer angles. With the increase of chamfer angle, both cutting force and axial force increased first and then decreased slightly, also the decrease amplitude was very small. When the chamfer angle was less than back rake angle, the influence of chamfer angle on cutting force and axial force was more obvious. When the chamfer angle was between 30° and 45°, the rock breaking process was relatively stable. With the increase of chamfer angle,

the maximum stress on the PDC cutter decreased gradually, and the distribution area of stress on the PDC cutter was wider, which was beneficial to protect the cutting edge, and prevent the occurrence of early cracks and spalls in the polycrystalline diamond layer of PDC cutter. The same results were obtained through drop hammer impact tests.

This work can provide a theoretical basis for the optimal design of chamfer parameters, future research will focus on studying the rock breaking effect of chamfered PDC cutters with different sizes ( $\Phi$  16 mm,  $\Phi$  19 mm), aiming to offer more comprehensive and perfect guidance for the optimization design of chamfer parameters. At the same time, field drilling test of PDC bit with different chamfered PDC cutters can be carried out, combined with the analysis of micro-morphology, the micro-mechanism of the chamfer on improving the impact resistance of the PDC cutter can be further revealed.

## Acknowledgements

This research was supported by Key Research and Development project in Shaanxi Province, grant number 2022GY-146, Science and Technology Innovation Fund Project of CCTEG Xi'an Research Institute, grant number 2021XAYJCQ02, and the National Key Research and Development project for young scientists, grant number 2021YFC2900200. I appreciate their support very much.

## References

- [1] Rajabov, V., Miska, S., Mortimer, L., Yu, M., Ozbayoglu, E. (2012). The effects of back rake and side rake angles on mechanical specific energy of single PDC cutters with selected rocks at varying depth of cuts and confining pressures, In: *Proceedings of the IADC/SPE Drilling Conference and Exhibition*, San Diego, California, USA, 1-17, [doi: 10.2118/151406-MS](https://doi.org/10.2118/151406-MS).
- [2] Zhang, Z., Zhao, D., Zhao, Y., Gao, K., Zhang, C., Lü, X. (2023). 3D numerical simulation study of rock breaking of the wavy PDC cutter and field verification, *Journal of Petroleum Science and Engineering*, Vol. 203, Article No. 108578, [doi: 10.1016/j.petrol.2021.108578](https://doi.org/10.1016/j.petrol.2021.108578).
- [3] Adzis, A.H.A., Abdul-Rani, A.M., Yi, K.Y., Maulianda, B.T., Rao, T.V.V.L.N. (2018). Effect of back rake angle and shape on wear rate of PDC cutter in hard formation, In: *Proceedings of the 6<sup>th</sup> International Conference on Production, Energy and Reliability, World Engineering Science & Technology Congress (ESTCON)*, Kuala Lumpur, Malaysia, 1-9, [doi: 10.1063/1.5075585](https://doi.org/10.1063/1.5075585).
- [4] Dai, X.-W., Huang, Z.-W., Huang, P.-J., Chen, P.-J., Shi, H.-Z., Yan, S. (2023). Experimental investigation on the cuttings formation process and its relationship with cutting force in single PDC cutter tests, *Petroleum Science*, Vol. 20, No. 3, 1779-1787, [doi: 10.1016/j.petsci.2022.10.021](https://doi.org/10.1016/j.petsci.2022.10.021).
- [5] Li, Y., Chen, Z., Ye, Y., Yang, Y. (2021). Combined finite-discrete element method for modeling the interaction between single PDC cutter and brittle rock, *Journal of Petroleum Science and Engineering*, Vol. 207, Article No. 109133, [doi: 10.1016/j.petrol.2021.109133](https://doi.org/10.1016/j.petrol.2021.109133).
- [6] Rahmani, R., Pastusek, P., Yun, G., Roberts, T. (2020). Investigation of geometry and loading effects on PDC cutter structural integrity in hard rocks, In: *Proceedings of the IADC/SPE International Drilling Conference and Exhibition*, Galveston, Texas, USA, 1-22, [doi: 10.2118/199598-MS](https://doi.org/10.2118/199598-MS).
- [7] Joodi, B., Sarmadivaleh, M., Rasouli, V., Nabipour, A. (2012). Simulation of the cutting action of a single PDC cutter using DEM, *Petroleum and Mineral Resources*, Vol. 81, 143-150, [doi: 10.2495/PMR120131](https://doi.org/10.2495/PMR120131).
- [8] Rostamsowlat, I., Akbari, B., Evans, B. (2018). Analysis of rock cutting process with a blunt PDC cutter under different wear flat inclination angles, *Journal of Petroleum Science and Engineering*, Vol. 171, 771-783, [doi: 10.1016/j.petrol.2018.06.003](https://doi.org/10.1016/j.petrol.2018.06.003).
- [9] Zhang, C., Wang, J., Ke, X., Feng, X., Yang, Y., Ren, H., Huang, Z. (2023). Experimental study on working mechanics of PDC bit with worn teeth, *Diamond & Abrasives Engineering*, Vol. 43, No. 1, 35-42.
- [10] Yang, Y., Xie, S., Cai, C., Cao, Y., Li, B. (2023). A study on the mechanism of heat generation law of PDC wear tooth cutting, *Journal of Southwest Petroleum University (Science & Technology Edition)*, Vol. 45, No. 1, 180-188, [doi: 10.11885/j.issn.1674-5086.2020.06.04.03](https://doi.org/10.11885/j.issn.1674-5086.2020.06.04.03).
- [11] Liu, W., Deng, H., Liu, Y., Chen, X., He, C., Zhu, X. (2023). Experimental investigation of the rock cutting process with blunt PDC cutters, *Geoenergy Science and Engineering*, Vol. 226, Article No. 211803, [doi: 10.1016/j.geoen.2023.211803](https://doi.org/10.1016/j.geoen.2023.211803).
- [12] Baker Hughes. StabilisX shaped-cutter technology, from <https://www.bakerhughes.com/drilling/drill-bits/shapedcutter-technology/stabilisx-shapedcutter-technology>, accessed July 28, 2023.
- [13] Shao, F., Liu, W., Gao, D. (2021). Effects of the chamfer and materials on performance of PDC cutters, *Journal of Petroleum Science and Engineering*, Vol. 205, Article No. 108887, [doi: 10.1016/j.petrol.2021.108887](https://doi.org/10.1016/j.petrol.2021.108887).
- [14] Fu, Z., Tergeist, M., Kueck, A., Ostermeyer, G.-P. (2022). Investigation of the cutting force response to a PDC cutter in rock using the discrete element method, *Journal of Petroleum Science and Engineering*, Vol. 213, Article No. 110330, [doi: 10.1016/j.petrol.2022.110330](https://doi.org/10.1016/j.petrol.2022.110330).



- [15] Akbari, B., Miska, S. (2016). The effects of chamfer and back rake angle on PDC cutters friction, *Journal of Natural Gas Science and Engineering*, Vol. 35, Part A, 347-353, doi: [10.1016/j.jngse.2016.08.043](https://doi.org/10.1016/j.jngse.2016.08.043).
- [16] Jamaludin, A.A., Mehat, N.M., Kamaruddin, S. (2019). Optimizing wear rate for PDC cutter using Taguchi's technique and response surface methodology a comparative analysis, *International Journal of Engineering & Technology*, Vol. 8, No. 3, 155-161.
- [17] Detournay, E., Defourny, P. (1992). A phenomenological model for the drilling action of drag bits, *International Journal of Rock Mechanics and Mining Sciences & Geomechanics Abstracts*, Vol. 29, No. 1, 13-23, doi: [10.1016/0148-9062\(92\)91041-3](https://doi.org/10.1016/0148-9062(92)91041-3).
- [18] Zhang, Z., Zhou, Q., Zhang, K., Zheng, G., Zhang, T. (2019). Analysis of the influence of rock cutting depth on the temperature distribution of cutter, *Journal of China Coal Society*, Vol. 44, No. S2, 492-501, doi: [10.13225/j.cnki.jccs.2019.0949](https://doi.org/10.13225/j.cnki.jccs.2019.0949).
- [19] Ju, P., Tian, D., Tian, H. (2023). Simulation and experimental study on rock disintegration characteristics of special-shaped PDC cutters, *Gazi University Journal of Science*, Vol. 36, No. 1, 414-428, doi: [10.35378/guis.927956](https://doi.org/10.35378/guis.927956).
- [20] Yahiaoui, M., Paris, J.-Y., Delbé, K., Denape, J., Gerbaud, L., Dourfaye, A. (2016). Independent analyses of cutting and friction forces applied on a single polycrystalline diamond compact cutter, *International Journal of Rock Mechanics & Mining Sciences*, Vol. 85, 20-26, doi: [10.1016/j.ijrmms.2016.03.002](https://doi.org/10.1016/j.ijrmms.2016.03.002).
- [21] Munoz, H., Taheri, A., Chanada, E. (2016). Rock cutting characteristics on soft-to-hard rocks under different cutter inclinations, *International Journal of Rock Mechanics and Mining Sciences*, Vol. 87, 85-89, doi: [10.1016/j.ijrmms.2016.05.014](https://doi.org/10.1016/j.ijrmms.2016.05.014).
- [22] Rostamsowlat, I., Richard, T., Evans, B. (2018). An experimental study of the effect of back rake angle in rock cutting, *International Journal of Rock Mechanics and Mining Sciences*, Vol. 107, 224-232, doi: [10.1016/j.ijrmms.2018.04.046](https://doi.org/10.1016/j.ijrmms.2018.04.046).
- [23] Zhu, X.H., Wang, Y.F., Liu, W.J., Tan, B., Luo, Y.X., Li, Z.L. (2023). A new method for evaluating the rock cutting and breaking performance of PDC cutters in heterogeneous granites, *Natural Gas Industry*, Vol. 43, No. 4, 137-147.
- [24] Ju, P., Tian, D., Wang, C., Tian, H. (2021). Theoretical and simulation analysis on rock breaking mechanical properties of arc-shaped PDC bit, *Energy Reports*, Vol. 7, 6690-6699, doi: [10.1016/j.egy.2021.09.148](https://doi.org/10.1016/j.egy.2021.09.148).
- [25] Mazen, A.Z., Rahmanian, N., Mujtaba, I.M., Hassanpour, A. (2021). Effective mechanical specific energy: A new approach for evaluating PDC bit performance and cutters wear, *Journal of Petroleum Science and Engineering*, Vol. 196, Article No. 108030, doi: [10.1016/j.petrol.2020.108030](https://doi.org/10.1016/j.petrol.2020.108030).
- [26] Xiong, C., Huang, Z.-W., Wang, L.-C., Shi, H.-Z., He, W.-H., Chen, Z.-L., Li, G.-S. (2023). Study on rock breaking characteristics and mechanism of conical PDC cutter, *Rock and Soil Mechanics*, Vol. 44, No. 8, 2432-2444.
- [27] Kenneth, E., Russell, S.C. (2016). Innovative ability to change drilling responses of a PDC bit at the rigsite using interchangeable depth-of-cut control features, In: *Proceedings of the IADC/SPE Drilling Conference and Exhibition*, Fort Worth, Texas, USA, 1-10, doi: [10.2118/178808-MS](https://doi.org/10.2118/178808-MS).
- [28] Wang, Y.L., Yang, L., Chen, J.H., Li, P. (2023). Supply chain game analysis based on mean-variance and price risk aversion under different power structures, *Advances in Production Engineering & Management*, Vol. 18, No. 1, 104-115, doi: [10.14743/apem2023.1.460](https://doi.org/10.14743/apem2023.1.460).
- [29] Ma, Y.C., Zhang, P., Huang, Z.Q., Deng, R., Yu, H.M. (2020). Optimal design for cutter-layout of global force balanced PDC bits, *China Mechanical Engineering*, Vol. 31, No. 20, 2412-2419, doi: [10.3969/j.issn.1004-132X.2020.20.003](https://doi.org/10.3969/j.issn.1004-132X.2020.20.003).
- [30] Liu, S.B., Ni, H.J., Wang, Y., Zhang, H. (2021). Mechanism of multi-dimensional impact loads applied in increasing the rock cutting efficiency of a PDC bit, *Journal of Vibration and Shock*, Vol. 40, No. 2, 258-264, doi: [10.13465/j.cnki.jvs.2021.02.035](https://doi.org/10.13465/j.cnki.jvs.2021.02.035).
- [31] Fakhimi, A., Lanari, M. (2014). DEM-SPH simulation of rock blasting, *Computers and Geotechnics*, Vol. 55, 158-164, doi: [10.1016/j.compgeo.2013.08.008](https://doi.org/10.1016/j.compgeo.2013.08.008).
- [32] Das, R., Cleary, P.W. (2010). Effect of rock shapes on brittle fracture using Smoothed Particle Hydrodynamics, *Theoretical and Applied Fracture Mechanics*, Vol. 53, No. 1, 47-60, doi: [10.1016/j.tafmec.2009.12.004](https://doi.org/10.1016/j.tafmec.2009.12.004).
- [33] Bennett, K.C., Regueiro, R.A., Luscher, D.J. (2019). Anisotropic finite hyper-elastoplasticity of geomaterials with Drucker-Prager/Cap type constitutive model formulation, *International Journal of Plasticity*, Vol. 123, 224-250, doi: [10.1016/j.ijplas.2018.11.010](https://doi.org/10.1016/j.ijplas.2018.11.010).
- [34] Huang, Z., Ma, Y., Li, Q., Xie, D. (2017). Geometry and force modelling, and mechanical properties study of polycrystalline diamond compact bit under wearing condition based on numerical analysis, *Advances in Mechanical Engineering*, Vol. 9, No. 6, 1-15, doi: [10.1177/1687814017702080](https://doi.org/10.1177/1687814017702080).